Chirality in Gold Nanoclusters Probed by NMR Spectroscopy

Huifeng Qian,[†] Manzhou Zhu,[‡] Chakicherla Gayathri,[†] Roberto R. Gil,[†,*] and Rongchao Jin[†,*]

[†]Department of Chemistry, Carnegie Mellon University, Pittsburgh, Pennsylvania 15213, United States and, [‡]Department of Chemistry, Anhui University, Hefei, Anhui 230026, People's Republic of China

ABSTRACT We report the analysis of chirality in atomically precise gold nanoclusters by nuclear magnetic resonance (NMR) spectroscopic probing of the surface ligands. The $Au_{38}(SR)_{24}$ and $Au_{25}(SR)_{18}$ (where, R = CH_2CH_2Ph) are used as representative models for chiral and nonchiral nanoclusters, respectively. Interestingly, different ^1H signals for the two germinal protons in each CH_2 of the ligands on the chiral $Au_{38}(SR)_{24}$ nanocluster were observed, so-called *diastereotopicity*. For α-CH_2 (closest to the chiral metal core), a chemical shift difference of up to ~0.8 ppm was observed. As for the nonchiral $Au_{25}(SCH_2CH_2Ph)_{18}^{-}TOA^{+}$ nanocluster, no diastereotopicity was detected (*i.e.*, no chemical shift difference for the two protons in the CH_2), confirming the Au_{25} core being nonchiral. These two typical examples demonstrate that NMR spectroscopy can be a useful tool for investigating chirality in Au nanoclusters. Since the diastereotopicity induced on the methylene protons by chiral nanoclusters is independent of the enantiomeric composition of the chiral particles, NMR can probe the chirality of the nanoclusters even in the case of a racemic mixture, while circular dichroism spectroscopy is not useful for racemic mixtures.

KEYWORDS: gold nanoclusters · chirality · NMR · diastereotopicity

Gold nanoclusters have received wide research interests due to their interesting structural and physicochemical properties[1−15] and promising applications in catalysis and other fields.[16−19] One of the major themes pertains to chiral Au nanoclusters.[20−29] Such nanoclusters are particularly attractive for enantioselective and stereoselective catalysis.[30−33] There are two general methods to impart chirality to ligand-protected Au nanoclusters. The first method is to functionalize nonchiral Au nanoclusters with chiral ligands, in which the chiral ligand can induce optical activity (*e.g.*, circular dichroism (CD) responses) in metal-based electronic transitions. The second method is to prepare intrinsically chiral Au nanoclusters (*i.e.*, chiral metal core). A long-standing major issue is how to verify the metal core chirality. In previous research, Schaaff and Whetten observed that the ultrasmall Au nanoclusters (~1 nm) protected by L-glutathione (GSH) showed strong optical CD activity.[20] Of those nanoclusters, the CD signal of $Au_{38}(SG)_{24}$ was found to be over 5 times stronger than that of $Au_{25}(SG)_{18}$.[20] Yao *et al.* prepared a pair of gold nanocluster enantiomers with D- and L-penicillamine ligands, which exhibited mirror-imaged optical CD signals.[34] Gautier *et al.* synthesized and separated a series of chiroptical gold nanoclusters with *N*-isobutyrl-L-cysteine and *N*-isobutyrl-D-cysteine.[35] Overall, in early research the total structure of Au nanoclusters had not been determined, thus, it was not clear if the optical activity of nanoclusters originated from the induction effect by chiral ligands or from the inherently chiral metal core.

Recent advances in the synthesis of thiolate-protected gold nanoclusters have led to a number of atomically monodisperse Au nanoclusters with size ranging from $Au_{20}(SR)_{16}$ to $Au_{144}(SR)_{60}$.[36−47] More importantly, the breakthroughs in total structure determinations of neutral $Au_{102}(p\text{-MBA})_{44}$ (p-MBA = p-mercaptobenzoic acid),[45] $[Au_{25}(SCH_2CH_2Ph)_{18}]^q$ (q = −1, 0),[48−50] and neutral $Au_{38}(SCH_2CH_2Ph)_{24}$ nanoclusters[51] have shed exciting light on the intriguing atomic packing structures of these nanoclusters and also opened up the possibility of correlating the chirality of Au nanoclusters with their atomic structures. Although the ligands (p-MBA and $PhCH_2CH_2SH$) are nonchiral, the metal cores of $Au_{102}(p\text{-MBA})_{44}$ and $Au_{38}(SCH_2CH_2Ph)_{24}$ nanoclusters were found to be inherently chiral, and each of them gives rise to a racemic pair in the crystal or solution.[45,51] The $Au_{102}(p\text{-MBA})_{44}$ possesses a kernel of 79 Au atoms (Au_{79}), which is nonchiral, but the $Au_{23}(p\text{-MBA})_{44}$ shell exhibits a chiral arrangement. The $Au_{23}(SR)_{44}$ shell can be divided into 19 monomeric staples of RS-Au-SR type (abbreviated as $Au(SR)_2$) and two dimeric staples of RS−Au−S(R)−Au−SR type (abbreviated as $Au_2(SR)_3$). The chirality of $Au_{102}(p\text{-MBA})_{44}$ arises from the geometry of the equatorial gold atoms and associated thiolates on the surface.[45] The $Au_{38}(SCH_2CH_2Ph)_{24}$ nanocluster is another nanocluster with

* Address correspondence to rgil@andrew.cmu.edu, rongchao@andrew.cmu.edu.

Received for review August 14, 2011 and accepted September 30, 2011.

Published online October 07, 2011
10.1021/nn203113j

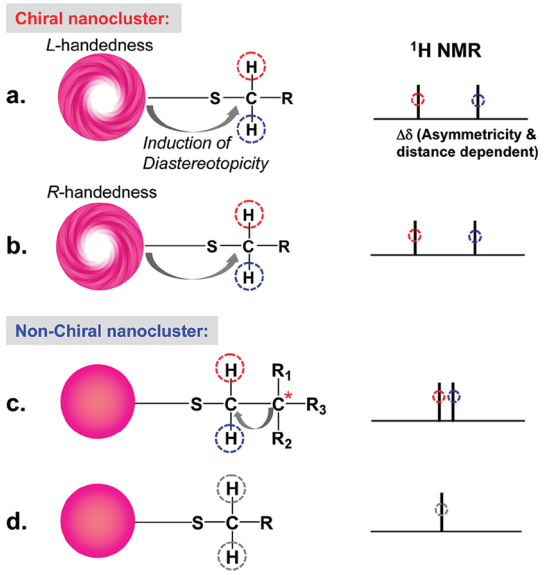

Scheme 1. Diastereotopicity in the CH_2 protons of the ligands on nanoclusters, (a,b) chiral metal-core-induced diastereotopicity, (c) chiral carbon-center-induced diastereotopicity, and (d) is an ordinary case

inherent chirality in the metal core. It contains a face-sharing biicosahedral Au_{23} kernel (resembling a rod) with D_{3h} symmetry and a $Au_{15}(SR)_{24}$ shell. The $Au_{15}(SR)_{24}$ shell consists of three $Au(SR)_2$ monomeric staples and six $Au_2(SR)_3$ dimeric staples. The chirality in $Au_{38}(SR)_{24}$ originates from the dual-propeller-like distribution of the six $Au_2(SR)_3$ dimeric staples on the Au_{23} rod, with one enantiomer exhibiting clockwise (*L*-) and the other anticlockwise (*R*-) arrangements.[51] In contrast, $[Au_{25}(SCH_2CH_2Ph)_{18}]^q$ comprises an icosahedral Au_{13} kernel and symmetric arrangement (D_{2h}) of six $Au_2(SR)_3$ dimeric staples and is nonchiral due to its plane symmetry,[48−50] but L-glutathione-capped $[Au_{25}(SG)_{18}]^-$ nanoclusters exhibit distinct CD signals in the metal-based electronic transition region due to induction by the chiral −SG ligands.[20,52]

To probe the internal chiral structure of Au nanoclusters, circular dichroism (CD) is a widely used method, but the racemic Au nanoclusters result in a net zero signal. Thus, the intrinsic chirality of racemic Au_{102} and Au_{38} nanoclusters could not be revealed until their crystal structures were determined recently.[45,51] The determination of the crystal structure of Au nanoclusters is, however, still very challenging, as it is very difficult to grow high-quality single crystals of Au nanoclusters. Therefore, it is highly desirable to find an analytical method that allows for probing the intrinsic chirality of nanoclusters, especially in racemic mixtures.

In this work, we demonstrate that NMR spectroscopy is capable of probing the nature of chiral nanoclusters using the diastereotopicity induced in the α-CH_2 protons of the ligand (Scheme 1). In organic chemistry, diastereotopic protons belonging to freely, fast

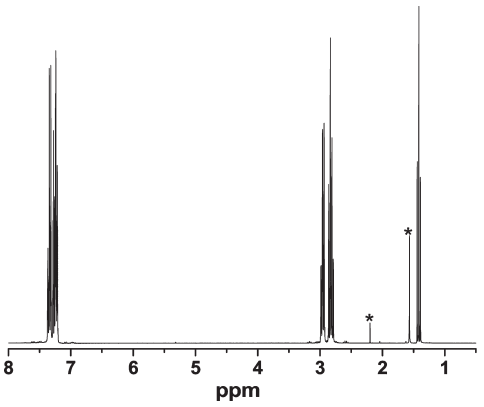

Figure 1. ^1H NMR spectrum of free $HSCH_2CH_2Ph$ in $CDCl_3$. The asterisks indicate solvent peaks.

rotating CH_2 groups attached to or in proximity to a chiral center do not show chemical equivalence in NMR spectroscopy. This phenomenon was first observed by Nair and Roberts back in 1957.[53] Herein, we use chiral $Au_{38}(SCH_2CH_2Ph)_{24}$ and nonchiral $Au_{25}(SCH_2CH_2Ph)_{18}^-TOA^+$ nanoclusters as model systems to learn how the ^1H NMR signals correlate with the nature of chirality in nanoclusters. Interestingly, $Au_{38}(SCH_2CH_2Ph)_{24}$ nanoclusters exhibit a large chemical shift difference in the protons of the α-CH_2 (an AB system with $\Delta\delta$ of up to ∼0.8 ppm), whereas $Au_{25}(SCH_2CH_2Ph)_{18}$ nanoclusters do not exhibit such an effect. To the best of our knowledge, this is the first report on the NMR chemical shift inequivalence of the CH_2 signal of the ligands (*i.e.*, diastereotopicity) induced by chiral Au nanoclusters. Of note, one should not confuse diastereotopicity with diasteromers, as the former refers to the CH_2 group of the ligand, rather than the metal core. The principle of diastereotopicity is quite simple yet highly effective for chirality analysis, as demonstrated in this work, and should be extendable and useful for future analysis on the chirality of nanoclusters, even in the presence of racemates; for the latter case, the CD spectroscopy apparently cannot provide useful information, albeit CD is a powerful tool for characterizing the separated enantiomers.[20,21,34]

RESULTS AND DISCUSSION

Before we discuss the detailed NMR results of Au_{38} and Au_{25} nanoclusters capped by $-SCH_2CH_2Ph$ ligands, it is worth presenting the spectrum of the free $HS-CH_2CH_2Ph$ ligand first (Figure 1). The peak assignments are simple. The ^1H signals ranging from ∼7.2 to 7.5 ppm (multiplet, 5H) are from the phenyl group, ∼2.9 ppm (triplet, 2H) corresponding to the α-CH_2 group (relative to the −SH group), ∼2.8 ppm (quartet, 2H) to the β-CH_2 group (second closest to −SH), and ∼1.4 ppm (triplet, 1H) to the −SH group. Below we discuss three typical cases of $Au_n(SR)_m$ nanoclusters. It should be pointed out that the nanoclusters (*e.g.*, Au_{38} and Au_{25}) investigated in this

work are of *molecular purity* (>99%, no detectable impurities by mass spectrometry and NMR). There is no issue of size distribution (*e.g.*, its influence on the variations in the chemical environment of $-CH_2$) since such nanoclusters are literally molecular compounds.

The Case of Chiral $Au_{38}(SCH_2CH_2Ph)_{24}$. The ^1H NMR spectrum of $Au_{38}(SCH_2CH_2Ph)_{24}$ cluster is shown in Figure 2. The peaks at 7.3−6.8 ppm correspond to protons of the phenyl groups and are split into two sets with a ratio of 2:1. The most intriguing signals are the seven peaks in the region of 4.2 to 2.7 ppm, which correspond to the α- and β-CH_2 groups (where α and β denote the positions relative to the sulfur atom). The area ratio of phenyl to methylene signals is 120H/96.5H (see Figure S1 in the Supporting Information; the number of phenyl protons are set to 120, 5H × 24(ligands) = 120H); the integrated 96.5 protons correspond well to the expected number of α and β protons in total (4H × 24 = 96H). Thus, all the signals of the 24 phenylethylthiolates in the $Au_{38}(SCH_2CH_2Ph)_{24}$ formula were found; no additional signals for other organic compounds were observed in the spectrum (except the solvent residual peak at 5.3 ppm), indicating high purity of the nanoclusters. The broadening and splitting in the α- and β-methylene groups reflect variations in chemical shift for ligands in different binding sites (or chemical environments). While the phenyl protons only fall into two sets (2:1), the methylene groups fall into multiple sets and are hard to sort out based solely upon the 1D spectrum due to the loss of *J*-coupling information caused by signal broadening. To obtain further information, we have acquired 2D spectra of the $Au_{38}(SCH_2CH_2Ph)_{24}$ nanoclusters, including through-bond $^1H-^1H$ correlation spectrum (COSY) and one-bond $^1H-^{13}C$ correlation spectrum (HSQC).

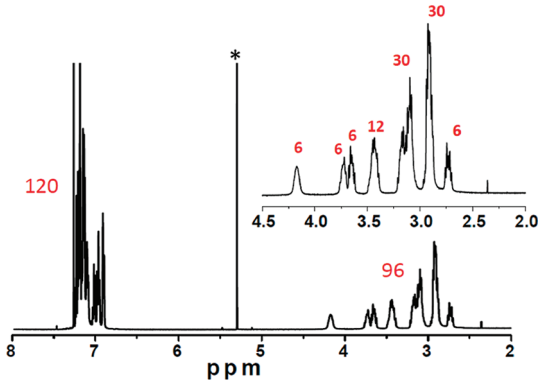

Figure 2. ^1H NMR spectrum of $Au_{38}(SCH_2CH_2Ph)_{24}$ in $CDCl_3$. Inset: zoom-in spectrum in the range of 4.5 to 2.0 ppm. The asterisk indicates the residual solvent signal. The proton numbers for the peaks are also shown (the phenyl protons are set to 120 according to the cluster formula).

In the HSQC spectrum (Figure 3A), the ^1H signals in the region 4.2−2.7 ppm show correlations with eight different carbons (see the ^{13}C dimension) at 34.8, 37.3, 39.1, 39.2, 40.8, 41.6, 42.4, and 42.6 ppm. Since each phenylethylthiolate has α- and β-CH_2 associated with two different carbons, the number of $-CH_2CH_2-$ sets is thus four (labeled **1** to **4** below), rather than two sets as indicated by the phenyl signals in the 1D spectrum (Figure 2). The latter is due to the fact that the phenyl groups are farther away from the Au_{38} core than the $-CH_2CH_2-$ groups, hence, the phenyl groups are not affected to the same extent as are $-CH_2CH_2-$ groups. Overall, the HSQC experiment reveals that the 24 $-SCH_2CH_2Ph$ ligands are exposed to four different chemical environments on the Au_{38} nanocluster. In addition, each carbon signal correlates with two different ^1H resonances, indicating that the two protons in each methylene group are not chemically equivalent. This is indeed due to the *diastereotopicity*

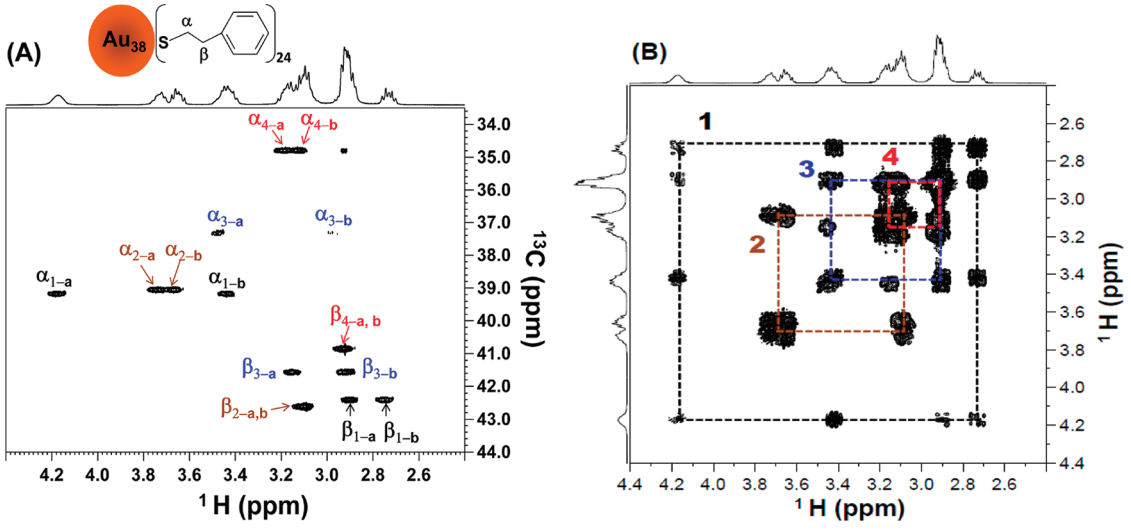

Figure 3. Two-dimensional NMR of $Au_{38}(SCH_2CH_2Ph)_{24}$ nanoclusters, (A) $^1H-^{13}C$ HSQC and (B) $^1H-^1H$ COSY. The α-CH_2 and β-CH_2 are as labeled (see the top of panel A); 1−4 denote the four sets of ligands; a and b represent each diastereotopic proton for each carbon (α- or β-CH_2) in the four sets of ligands.

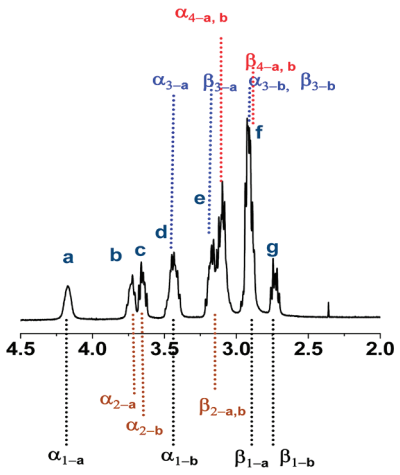

Figure 4. Full assignment of methylene protons in ^{1}H NMR spectrum of $Au_{38}(SCH_2CH_2Ph)_{24}$.

created on the methylene protons by the chiral Au_{38} core. The ^{1}H and ^{13}C resonances corresponding to the methylene groups can be assigned using the COSY and the HSQC experiments as discussed below.

The COSY spectrum was used to sort out the α-CH_2 and β-CH_2 sets based on the germinal ($^2J_{HH}$, through *two* bonds) and vicinal ($^3J_{HH}$, through *three* bonds) *J*-coupled hydrogen atoms, which are manifested by cross-correlation peaks off the diagonal in the 2D spectrum. We focus our analysis on the 2.4−4.4 ppm region (for full range spectra, see Figure S2) as this region is the most interesting one. Since α-CH_2 is closer to the gold core than β-CH_2, α-CH_2 should experience a larger *downfield* shift than β-CH_2. The left-most peak at 4.18 ppm (labeled as set **1**) is assigned to α_1 (*i.e.*, the α protons of set **1** ligands, integral: 6H). This 4.18 ppm resonance shows cross-peaks with the resonances at 3.42, 2.92, and 2.75 ppm in COSY (Figure 3B). According to HSQC, the ^{1}H resonances at 4.18 and 3.42 ppm belong to the same carbon (39.2 ppm, Figure 3A); thus, these two ^{1}H resonances are from diastereotopic protons attached to the same carbon (α_1-C**H$_2$**) and accordingly are labeled as $\alpha_{1\text{-a}}$ and $\alpha_{1\text{-b}}$ (Figure 3A). The remaining peaks at 2.92 and 2.75 ppm correspond to the protons attached to the vicinal carbon (42.4 ppm, β_1-C**H$_2$**), thus, labeled as $\beta_{1\text{-a}}$ and $\beta_{1\text{-b}}$, respectively, in the HSQC spectrum (Figure 3A). Up to this point, we have assigned the $-CH_2CH_2-$ protons of set **1**. For the sets of **2**−**4**, their α- and β-CH_2 can be assigned similarly (see labels in Figure 3A), and the 1D spectrum is fully assigned as shown in Figure 4.

Among the four sets of $-CH_2CH_2-$, set **1** shows the largest difference in chemical shift of the two diastereotopic protons attached to α_1-carbon ($\Delta\delta = \alpha_{1\text{-a}} - \alpha_{1\text{-b}} = 0.8$ ppm, Figure 3A), followed by the set **3** ($\Delta\delta \sim 0.6$ ppm), while the sets of **2** and **4** show a much smaller difference ($\Delta\delta \sim 0.1$ ppm for both α_2- and α_4-CH_2). Since the chemical shift difference ($\Delta\delta$) is dependent on the distance between the CH_2 group

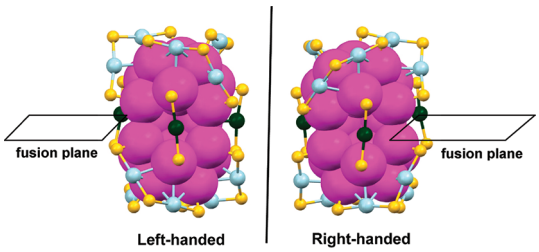

Figure 5. Atomic packing structures of the two enantiomers of $Au_{38}(SCH_2CH_2Ph)_{24}$ nanoclusters. Color labels: yellow, S; all other colors are for Au atoms in different positions.

and the chiral center (Scheme 1), the $\Delta\delta$ value for the diastereotopic protons in β-CH_2 is expected to be smaller than that of the α-CH_2 of the *same* set of ligands, which is indeed as observed (Figure 3A); for example, for β_1-CH_2, $\Delta\delta = \beta_{1\text{-a}} - \beta_{1\text{-b}} = 2.9 - 2.75 = 0.15$ ppm, much smaller than the 0.8 ppm ($\Delta\delta$) for the α_1-CH_2. In our previous work, we once observed the difference in the ^{1}H chemical shift of the methylene protons in L-glutathione on $Au_{25}(SG)_{18}$ nanoclusters,[52] but in that case, the diastereotopicity was induced by the chiral carbon (Scheme 1c), rather than the Au_{25} metal core. Thus, the present work is the first time it was observed that the inherently chiral Au nanoclusters cause a large chemical shift difference ($\Delta\delta$ up to 0.8 ppm) in the NMR resonances of α-methylene protons.

Following the diastereotopicity analysis above, we next proceed to correlate the NMR results with the structure of $Au_{38}(SCH_2CH_2Ph)_{24}$. In the unit cell of the $Au_{38}(SCH_2CH_2Ph)_{24}$ crystal structure, the nanoclusters exist in a pair of enantiomers (Figure 5, CH_2CH_2Ph omitted for clarity).[51] The Au_{23} kernel in $Au_{38}(SCH_2CH_2Ph)_{24}$ consists of two icosahedrons fused together by sharing a common triangular face (*i.e.*, 13 + 13 − 3 = 23) and is in D_{3h} symmetry. The chirality of $Au_{38}(SCH_2CH_2Ph)_{24}$ indeed arises from the dual-propeller-like rotative distribution of the six $Au_2(SCH_2CH_2Ph)_3$ dimeric staples: one particle is left-handed, and the other is right-handed (Figure 5). The above NMR analysis has revealed four sets of ligands in the structure of $Au_{38}(SCH_2CH_2Ph)_{24}$, and the ratio of the four sets of ligands can be determined by their peak areas. The integrals of the seven ^{1}H peaks (**a**−**g**) from methylene groups (ranging from 4.2 to 2.7 ppm) are 6, 6, 6, 12, 30, 30, and 6, respectively (Figure S1). Since there are 16 groups of methylene protons ($\alpha_{n\text{-a}}$, $\alpha_{n\text{-b}}$, $\beta_{n\text{-b}}$, $\beta_{n\text{-b}}$, each *n* takes 1 to 4), some of the 7 peaks apparently contain two or more proton groups (*i.e.*, overlapped). When calculating the proton number in each set of ligands (**1**−**4**), we apply the following restrictions: (1) the proton number in α_n-CH_2 should be equal to that in β_n-CH_2 of the same set (*n*), and (2) the diastereotopic protons must be $\alpha_{n\text{-a}} = \alpha_{n\text{-b}}$ and $\beta_{n\text{-a}} = \beta_{n\text{-b}}$. Under these restrictions, one can work out the proton numbers of α-CH_2 and β-CH_2 in the four sets of ligands

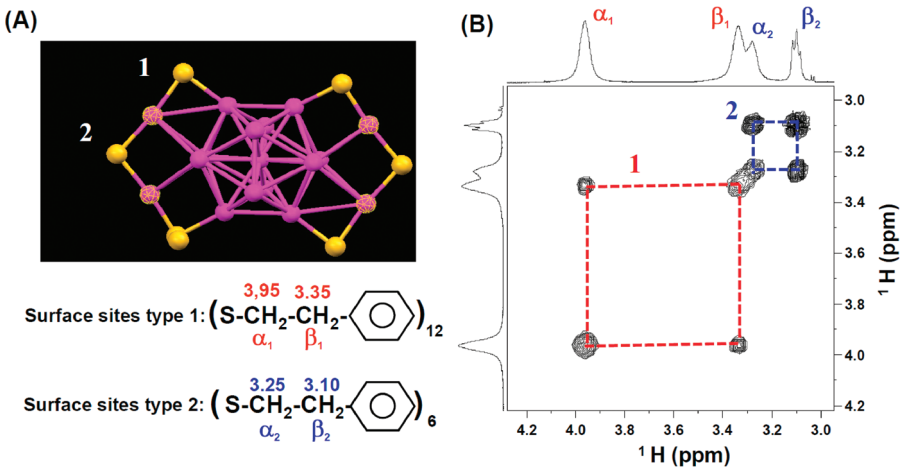

Figure 6. (A) Partial structure of $Au_{25}(SCH_2CH_2Ph)_{18}^-TOA^+$ (CH_2CH_2Ph groups are omitted). Purple, Au atoms; yellow, sulfur atom. The chemical shifts of methylene protons of set 1 (interior sites) and set 2 (exterior sites) are listed. (B) $^1H-^1H$ COSY spectrum acquired in toluene-d_8.

(Table S1) and further calculate the ratios of the four sets of ligands. From Table S1, we obtain the result $\alpha_{n\text{-a}} = \alpha_{n\text{-b}} = \beta_{n\text{-a}} = \beta_{n\text{-b}} = 6H$ (n = 1, 2, 3, 4). Thus, each set possesses six ligands, and the total number of ligands is 4(set) × 6(ligand per set) = 24 ligands, which is as expected.

The four sets of ligands indicate that there are four different chemical environments for the surface ligands on Au_{38}. As shown in Figure 5, the 24 ligands comprise 6 dimeric staples ($Au_2(SR)_3$) and 3 monomeric staples ($Au(SR)_2$). The −SR ligands above the fusion plane are chemically equivalent with those below the fusion plane (Figure 5), thus we only need to consider half of the structure (*e.g.*, the portion above the fusion plane). In the half structure, one end of each of the dimeric staples (−SR−Au−SR−Au−SR−) binds to the Au atom at the Au_{23} rod's end, and the other end of the dimeric staple binds to the Au atom near the fusion plane. Thus, the three −SR ligands in each dimeric staple are in three chemical environments, and the dimeric staples give rise to three sets of distinct −SR ligands: $-SR_{1'}-Au-SR_{2'}-Au-SR_{3'}-$, and each set has six ligands (three on the top icosahedron and another three at the bottom icosahedron). The fourth set of ligands comes from the monomeric staples (Figure 5), which comprises 6 −SR ligands in total (note, each monomeric staple contains two ligands). Therefore, the NMR results of four sets of ligands (each set with 6 ligands) are consistent with the crystal structure of the chiral $Au_{38}(SCH_2CH_2Ph)_{24}$ nanoclusters. But we are still not able to match **1**−**4** with **1′**−**4′**, respectively; for this task, theoretical calculations[29] of the NMR signals are needed.

Given the metal core chirality-induced diastereotopicity on the CH_2 of the ligands, one may wish to compare achiral Au_{38} with chiral Au_{38} stabilized by the same ligand in order to consolidate the conclusion that the NMR technique can indeed be used for determining the chirality in nanoclusters. Unfortunately, the Au_{38} clusters made thus far are chiral. We have no clue that nonchiral Au_{38} clusters would exist. Nature chooses the chiral configuration as the *most stable* structure for Au_{38} clusters; indeed, DFT calculations have confirmed that the chiral configuration is more stable (hence, experimentally made in the synthesis) than the nonchiral Au_{38} structure.[15,25] In consideration of that, we next use nonchiral Au_{25} clusters as a model to further demonstrate that NMR spectroscopy is indeed a very useful technique for probing chirality in nanoclusters (*vide infra*).

The Case of Nonchiral $Au_{25}(SCH_2CH_2Ph)_{18}^-TOA^+$. In order to compare the difference(s) between chiral Au nanoclusters and nonchiral ones, we have also studied the 1D and 2D NMR spectra of nonchiral $Au_{25}(SCH_2CH_2Ph)_{18}^-TOA^+$. About 10 mg of $Au_{25}(SCH_2CH_2Ph)_{18}^-TOA^+$ was dissolved in solvent (toluene-d_8) for ^1H NMR measurement. Figure S3 (Supporting Information) shows the ^1H NMR spectrum of $Au_{25}(SCH_2CH_2Ph)_{18}^-TOA^+$. The proton peaks at 2.8, 1.4, and 0.9 ppm are from the counterion $[CH_3(CH_2)_6CH_2]_4N^+$ (abbreviated TOA^+),[54−56] with the 2.8 ppm peak corresponding to the $^+N-CH_2$ in TOA^+ (expected, 8H; integral, 8H), 1.4 ppm to the six $-CH_2-$ groups (expected, 48H; integral, ~50H), and 0.9 ppm to the $-CH_3$ group (expected, 12H; integral, ~12H), Figure S3. The COSY spectrum (Figure S4) also confirms the above assignment.

Here, we focus on the region of 4.2−3 ppm in the ^1H NMR spectrum (Figure 6): the peaks at 3.95, 3.35, 3.25, and 3.10 ppm arise from the methylene groups in the $PhCH_2CH_2S-$ ligands. According to the COSY spectrum (Figure 6B), the proton peaks at 3.95 and 3.35 ppm are from one set of ligands (labeled as set **1**) and those at 3.25 and 3.10 ppm from another set of ligands (labeled as set **2**). Considering the influence from the Au core, the proton peak of α-CH_2 should shift more downfield than that of β-CH_2. Therefore, the proton peak at

3.95 ppm is attributed to α-CH_2 of set **1** and the 3.35 ppm peak to β-CH_2 of set **1**. Similarly, the proton peaks at 3.25 and 3.10 ppm are attributed to α-CH_2 and β-CH_2 of set **2**, respectively. The ratio of ligand set **1** to **2** can be calculated from the integrals of α_1-CH_2 and β_2-CH_2 (note, β_1 and α_2 are overlapped), which is 24:12 = 2:1. Taken together, there are two sets of $PhCH_2CH_2S-$ ligands with distinct chemical environments, and their ratio is 2:1. The structure of $Au_{25}(SCH_2CH_2Ph)_{18}^-TOA^+$ contains an icosahedral Au_{13} kernel and six dimeric staples ($-SR-Au-SR-Au-SR-$; see the partial structure shown in Figure 6A). Apparently, there are two distinct chemical environments for the 18 ligands,[52,54−57] corresponding to the interior site (assigned as set **1**) and the exterior site (set **2**), and their ratio is 2:1, consistent with the NMR result. Due to the larger influence from the Au_{13} kernel, the proton peak for the interior set **1** shows a more significant downfield shift compared to the ligand set **2** at the exterior binding site.

Unlike $Au_{38}(SCH_2CH_2Ph)_{24}$, no diastereotopic signals of protons in the CH_2 of the ligands are observed in the $Au_{25}(SCH_2CH_2Ph)_{18}^-TOA^+$ nanocluster, indicating that the Au_{25} metal core framework is nonchiral. Similarly, the charge-neutral $[Au_{25}(SCH_2CH_2Ph)_{18}]^0$ nanocluster is also nonchiral, as indicated in the NMR spectrum.[50] Very recently, pure $[Au_{25}(SCH_2CH_2Ph)_{18}]^+$ nanoclusters have been prepared through the controlled oxidation processes, and NMR analyses of the cationic nanocluster show a similar NMR spectrum as that of the anionic form.[55,56] According to the diastereotopicity principle discussed above, we conclude that the $[Au_{25}(SCH_2CH_2Ph)_{18}]^q$ ($q = -1, 0, +1$) nanoclusters are all nonchiral regardless of the charge state, rather than a racemic mixture speculated by some researchers. This conclusion is also supported by the crystal structures of the anionic and neutral $Au_{25}(SCH_2CH_2Ph)_{18}$ (although the structure of its cationic form has not been attained thus far), in which no mirror-imaged structures were found in the unit cells;[49,50] in contrast, a pair of mirror-imaged particles was present in the unit cell of $Au_{38}(SCH_2CH_2Ph)_{24}$.[51]

The Case of $Au_{25}(SR^*)_{18}$ with Chiral Thiolate Ligands. The above sections have discussed the two scenarios pertinent to the chirality in the metal core of the nanocluster. Another interesting scenario is the nonchiral metal core but with chiral thiolate ligands, such as glutathione-capped $Au_{25}(SG)_{18}$ nanoclusters. Unlike $Au_{25}(SCH_2H_2Ph)_{18}$ that shows a null CD signal,[52] the $Au_{25}(SG)_{18}$ nanoclusters exhibit distinct CD signals: two prominent positive bands at 375 and 500 nm as well as two weak negative bands at 310 and 425 nm.[20,52] In our previous work, we confirmed that $Au_{25}(SG)_{18}$ nanoclusters adopt the same structure as that of $Au_{25}(SCH_2CH_2Ph)_{18}$.[52] The 18 ligands in the $Au_{25}(SG)_{18}$ nanocluster were found to exhibit two chemically inequivalent sets. The chiral carbon center (*e.g.*, C*-6, see Figure 2 in ref 52) in the $-SG$ ligand causes the ^1H NMR signal differences in the two protons of $-SC\mathbf{H}_2-$ ($\Delta\delta \sim 0.2$ ppm) due to diastereotopicity. This observation corresponds to the scenario shown in Scheme 1 (case c).

In our recent work,[58] we have also designed chirally modified phenylethylthiols at the 2-position, that is, HS-CH_2C*H(Me)Ph (abbreviated as pet*, *R*- and *S*-isomers). With these chiral ligands, we have successfully prepared $Au_{25}(R\text{-pet}^*)_{18}$ and $Au_{25}(S\text{-pet}^*)_{18}$ nanoclusters.[58] These two types of $Au_{25}(pet^*)_{18}$ nanoclusters exhibit mirror-imaged CD signals. Such optically active $Au_{25}(pet^*)_{18}$ nanoclusters are close analogues of the optically *nonactive* $Au_{25}(SCH_2CH_2Ph)_{18}$ nanoclusters and share the same metal core structure as the crystallographically characterized $Au_{25}(SCH_2CH_2Ph)_{18}$. On the basis of the atomic and electronic structures of these well-defined Au_{25} nanoclusters, we have explicitly revealed that the ligand and surface gold atoms of $Au_{25}(pet^*)_{18}$ play a critical role in effecting the CD responses from the nanoclusters. The cluster's CD signals are due to induction by chiral $-SG$ or $-pet^*$ ligands (*i.e.*, electronic state mixing). This induction effect strongly affects those electronic transitions involving surface gold atoms and ligands (such as the $\sim$400 and $\sim$450 nm absorption peaks in the UV−vis absorption spectrum) but barely affects the HOMO−LUMO transition of $Au_{25}(SR^*)_{18}$ at $\sim$670 nm since the latter transition occurs primarily in the Au_{13} icosahedral kernel.

As for the $Au_{25}(SCH_2CH_2Ph)_{18}$ clusters, since the Au_{25} metal core is nonchiral, there is no diastereotopicity on the α-CH_2 and β-CH_2. In contrast with $Au_{25}(SG)_{18}$ clusters that show distinct CD signals, the null CD signal of $Au_{25}(SCH_2CH_2Ph)_{18}$ is not due to a racemic mixture but due to $Au_{25}(SCH_2CH_2Ph)_{18}$ being nonchiral. Moreover, since anionic and neutral $Au_{25}(pet^*)_{18}$ nanoclusters showed comparable intensities of CD signals, the small structural distortions in the anionic cluster should not be the origin of observed CD signals. Finally, recent NMR studies of $[Au_{25}(SCH_2CH_2Ph)_{18}]^q$ ($q = -1, 0, +1$) clusters by Maran and co-workers[55] and by Zhu *et al.*[56] showed no diastereotopicity in $[Au_{25}(SCH_2CH_2Ph)_{18}]^q$ nanoclusters regardless of TOA^+ counterions being present or not in the solution.

To summarize the third scenario, nonchiral Au_{25} core with chiral ligands such as $Au_{25}(SG)_{18}$ and $Au_{25}(pet^*)_{18}$, our conclusion is that the Au_{25} metal core does not cause diastereotopicity in nearby CH_2 groups since the metal core is nonchiral, but the chiral center(s) in the ligand itself can induce diastereotopicity in the CH_2. As long as there is a chiral center (regardless of a chiral carbon or a chiral metal cluster core) connected to the CH_2 group, one will observe diastereotopicity in this CH_2 group, and the general rule is that the closer the CH_2 group is to the chiral center, the stronger the diastereotopicity will be.

CONCLUSION

In this work, NMR spectroscopy is demonstrated to successfully probe the chirality of well-defined Au nanoclusters. The chiral $Au_{38}(SCH_2CH_2Ph)_{24}$ and nonchiral $Au_{25}(SCH_2CH_2Ph)_{18}^-TOA^+$ nanoclusters are used as examples of chiral and nonchiral gold nanoclusters, respectively. The chiral $Au_{38}(SCH_2CH_2Ph)_{24}$ shows a distinct ^1H signal for each individual proton in both the α- and β-CH_2 groups of the ligands. For the α-CH_2, a large difference of up to ~0.8 ppm was observed in the chemical shift of each germinal proton. Such differences in chemical shift are caused by the chiral Au_{38} metal framework. In contrast, in the case of the nonchiral $Au_{25}(SCH_2CH_2Ph)_{18}$ nanocluster, the two protons of each CH_2 group are chemically equivalent. On the basis of these results, NMR spectroscopy is a very useful method for studying the inherent chirality of atomically monodisperse Au nanoclusters. It is important to highlight that the diastereotopicity induced on the methylene protons by the chirality of the nanoclusters is independent of the enantiomeric composition of the chiral particles. Hence, the chirality of the nanoclusters can be successfully probed even in the presence of a racemic mixture, which is a significant advantage over the routinely used circular dichroism spectroscopic method for the analysis of chiral nanoclusters.

METHODS

Synthesis and Crystallization of $Au_{38}(SCH_2CH_2Ph)_{24}$ and $Au_{25}(SCH_2CH_2Ph)_{18}^-TOA^+$ Nanoclusters. The synthesis of atomically precise $Au_{38}(SCH_2CH_2Ph)_{24}$ and $Au_{25}(SCH_2CH_2Ph)_{18}^-TOA^+$ (TOA^+ = tetra-*n*-octylammonium) nanoclusters was reported in previous work.[44,49] Crystallization was done in toluene/ethanol (1:2 for $Au_{38}(SCH_2CH_2Ph)_{24}$ and 1:4 for $Au_{25}(SCH_2CH_2Ph)_{18}^-TOA^+$).[49,51] The dark crystals of nanoclusters were collected and used in NMR after redissolving in deuterated solvents.

Characterization. Nuclear magnetic resonance (NMR) analysis was performed on a Bruker Avance 500 spectrometer operating at 500.13 MHz for ^1H and 125.77 MHz for ^{13}C. For data collection, ~10 mg of $Au_{38}(SCH_2CH_2Ph)_{24}$ nanoclusters was dissolved in $CDCl_3$ and ~10 mg of $Au_{25}(SCH_2CH_2Ph)_{18}^-TOA^+$ nanoclusters was dissolved in toluene-d_8. The following experiments were performed for NMR analysis and signal assignment: 1D ^1H NMR, 2D correlation spectroscopy (COSY), and (^1H,^{13}C) heteronuclear single quantum correlation spectroscopy (HSQC).

Acknowledgment. This material is based upon work supported by the Air Force Office of Scientific Research under AFOSR Award No. FA9550-11-1-9999 (FA9550-11-1-0147) and the Camille Dreyfus Teacher-Scholar Awards Program. M.Z. acknowledges NSFC (20871112). NMR instrumentation at CMU was partially supported by NSF (CHE-0130903 and CHE-1039870). R.J. is a Camille Dreyfus Teacher-Scholar.

Supporting Information Available: ^1H NMR spectrum of $Au_{38}(SCH_2CH_2Ph)_{24}$ with integrals; 2D NMR of $Au_{38}(SCH_2CH_2Ph)_{24}$ nanoclusters in the full range; the assignment of methylene groups in ^1H NMR spectrum of $Au_{38}(SCH_2CH_2Ph)_{24}$; ^1H NMR and COSY spectrum of $Au_{25}(SCH_2CH_2Ph)_{18}^-TOA^+$. This material is available free of charge *via* the Internet at http://pubs.acs.org.

REFERENCES AND NOTES

1. Jin, R.; Zhu, Y.; Qian, H. Quantum Sized Gold Nanoclusters: Bridging the Gap between Organometallics and Nanocrystals. *Chem.—Eur. J.* **2011**, *17*, 6584–6593.
2. Whetten, R. L.; Shafigullin, M. N.; Khoury, J. T.; Schaaff, T. G.; Vezmar, I.; Alvarez, M. M.; Wilkinson, A. Crystal Structures of Molecular Gold Nanocrystal Arrays. *Acc. Chem. Res.* **1999**, *32*, 397–406.
3. Murray, R. W. Nanoelectrochemistry: Metal Nanoparticles, Nanoelectrodes, and Nanopores. *Chem. Rev.* **2008**, *108*, 2688–2720.
4. Tsukuda, T.; Tsunoyama, H.; Sakurai, H. Aerobic Oxidations Catalyzed by Colloidal Nanogold. *Chem. Asian J.* **2011**, *6*, 736–748.
5. Smith, R. K.; Nanayakkara, S. U.; Woehrle, G. H.; Pearl, T. P.; Blake, M. M.; Hutchison, J. E.; Weiss, P. S. Spectral Diffusion in the Tunneling Spectra of Ligand-Stabilized Undecagold Clusters. *J. Am. Chem. Soc.* **2006**, *128*, 9266–9267.
6. MacDonald, M. A.; Zhang, P.; Chen, N.; Qian, H.; Jin, R. Solution-Phase Structure and Bonding of $Au_{38}(SR)_{24}$ Nanoclusters from X-ray Absorption Spectroscopy. *J. Phys. Chem. C* **2011**, *115*, 65–69.
7. Quinn, B. M.; Liljeroth, P.; Ruiz, V.; Laaksonen, T.; Kontturi, K. Electrochemical Resolution of 15 Oxidation States for Monolayer Protected Gold Nanoparticles. *J. Am. Chem. Soc.* **2003**, *125*, 6644–6645.
8. Antonello, S.; Holm, A. H.; Instuli, E.; Maran, F. Molecular Electron-Transfer Properties of Au_{38} Clusters. *J. Am. Chem. Soc.* **2007**, *129*, 9836–9837.
9. Tang, Z.; Xu, B.; Wu, B.; Germann, M. W.; Wang, G. Synthesis and Structural Determination of Multidentate 2,3-Dithiol-Stabilized Au Clusters. *J. Am. Chem. Soc.* **2010**, *132*, 3367–3374.
10. Pettibone, J. M.; Hudgens, J. W. Gold Cluster Formation with Phosphine Ligands: Etching as a Size-Selective Synthetic Pathway for Small Clusters? *ACS Nano* **2011**, *5*, 2989–3002
11. Knoppe, S.; Boudon, J.; Dolamic, I.; Dass, A.; Burgi, T. Size Exclusion Chromatography for Semipreparative Scale Separation of $Au_{38}(SR)_{24}$ and $Au_{40}(SR)_{24}$ and Larger Clusters. *Anal. Chem.* **2011**, *83*, 5056–5061.
12. Woehrle, G. H.; Brown, L. O.; Hutchison, J. E. Thiol-Functionalized, 1.5-nm Gold Nanoparticles through Ligand Exchange Reactions: Scope and Mechanism of Ligand Exchange. *J. Am. Chem. Soc.* **2005**, *127*, 2172–2183.
13. Sardar, R.; Shumaker-Parry, J. S. Spectroscopic and Microscopic Investigation of Gold Nanoparticle Formation: Ligand and Temperature Effects on Rate and Particle Size. *J. Am. Chem. Soc.* **2011**, *133*, 8179–8190.
14. Jiang, D.; Whetten, R. L. Magnetic Doping of a Thiolated-Gold Superatom: First-Principles Density Functional Theory Calculations. *Phys. Rev. B* **2009**, *80*, 115402–115405.
15. Pei, Y.; Gao, Y.; Zeng, X. C. Structural Prediction of Thiolate-Protected Au_{38}: A Face-Fused Bi-icosahedral Au Core. *J. Am. Chem. Soc.* **2008**, *130*, 7830–7832.
16. Zhu, Y.; Qian, H.; Jin, R. Catalysis Opportunities of Atomically Precise Gold Nanoclusters. *J. Mater. Chem.* **2011**, *21*, 6793–6799.
17. Zhu, Y.; Qian, H.; Drake, B. A.; Jin, R. Atomically Precise $Au_{25}(SR)_{18}$ Nanoparticles as Catalysts for the Selective Hydrogenation of α,β-Unsaturated Ketones and Aldehydes. *Angew. Chem., Int. Ed.* **2010**, *49*, 1295–1298.
18. Chen, W.; Chen, S. Oxygen Electroreduction Catalyzed by Gold Nanoclusters: Strong Core Size Effects. *Angew. Chem., Int. Ed.* **2009**, *48*, 4386–4389.
19. Shao, M. H.; Peles, A.; Shoemaker, K.; Gummalla, M.; Njoki, P. N.; Luo, J.; Zhong, C. J. Enhanced Oxygen Reduction Activity of Platinum Monolayer on Gold Nanoparticles. *J. Phys. Chem. Lett.* **2011**, *2*, 67–72.
20. Schaaff, T. G.; Whetten, R. L. Giant Gold−Glutathione Cluster Compounds: Intense Optical Activity in Metal-Based Transitions. *J. Phys. Chem. B* **2000**, *104*, 2630–2641.

21. Gautier, C.; Burgi, T. Chiral Gold Nanoparticles. *ChemPhysChem* **2009**, *10*, 483–492.
22. Noguez, C.; Garzon, I. L. Optically Active Metal Nanoparticles. *Chem. Soc. Rev.* **2009**, *38*, 757–771.
23. Yanagimoto, Y.; Negishi, Y.; Fujihara, H.; Tsukuda, T. Chiroptical Activity of BINAP-Stabilized Undecagold Clusters. *J. Phys. Chem. B* **2006**, *110*, 11611–11614.
24. Knoppe, S.; Dharmaratne, A. C.; Schreiner, E.; Dass, A.; Burgi, T. Ligand Exchange Reactions on Au_{38} and Au_{40} Clusters: A Combined Circular Dichroism and Mass Spectrometry Study. *J. Am. Chem. Soc.* **2010**, *132*, 16783–16789.
25. Lopez-Acevedo, O.; Tsunoyama, H.; Tsukuda, T.; Hakkinen, H.; Aikens, C. M. Chirality and Electronic Structure of the Thiolate-Protected Au_{38} Nanocluster. *J. Am. Chem. Soc.* **2010**, *132*, 8210–8218.
26. Gautier, C.; Burgi, T. Chiral Inversion of Gold Nanoparticles. *J. Am. Chem. Soc.* **2008**, *130*, 7077–7084.
27. Yao, H.; Fukui, T.; Kimura, K. Asymmetric Transformation of Monolayer-Protected Gold Nanoclusters *via* Chiral Phase Transfer. *J. Phys. Chem. C* **2008**, *112*, 16281–16285.
28. Sanchez-Castillo, A.; Noguez, C.; Garzon, I. L. On the Origin of the Optical Activity Displayed by Chiral-Ligand-Protected Metallic Nanoclusters. *J. Am. Chem. Soc.* **2010**, *132*, 1504–1505.
29. Perera, N. V.; Isley, W.; Maran, F.; Gascon, J. A. Molecular Modeling Characterization of a Conformationally Constrained Monolayer-Protected Gold Cluster. *J. Phys. Chem. C* **2010**, *114*, 16043–16050.
30. Tamura, M.; Fujihara, H. Chiral Bisphosphine BINAP-Stabilized Gold and Palladium Nanoparticles with Small Size and Their Palladium Nanoparticle-Catalyzed Asymmetric Reaction. *J. Am. Chem. Soc.* **2003**, *125*, 15742–15743.
31. Corma, A.; Serna, P. Chemoselective Hydrogenation of Nitro Compounds with Supported Gold Catalysts. *Science* **2006**, *313*, 332–334.
32. Shukla, N.; Bartel, M. A.; Gellman, A. J. Enantioselective Separation on Chiral Au Nanoparticles. *J. Am. Chem. Soc.* **2010**, *132*, 8575–8580.
33. Zhu, Y.; Wu, Z.; Gayathri, C.; Qian, H.; Gil, R. R.; Jin, R. Exploring Stereoselectivity of Au_{25} Nanoparticle Catalyst for Hydrogenation of Cyclic Ketone. *J. Catal.* **2010**, *271*, 155–160.
34. Yao, H.; Fukui, T.; Kimura, K. Chiroptical Responses of D-/L-Penicillamine-Capped Gold Clusters under Perturbations of Temperature Change and Phase Transfer. *J. Phys. Chem. C* **2007**, *111*, 14968–14976.
35. Gautier, C.; Burgi, T. Chiral *N*-Isobutyryl-Cysteine Protected Gold Nanoparticles: Preparation, Size Selection, and Optical Activity in the UV–Vis and Infrared. *J. Am. Chem. Soc.* **2006**, *128*, 11079–11087.
36. Zhu, M.; Qian, H.; Jin, R. Thiolate-Protected Au_{20} Clusters with a Large Energy Gap of 2.1 eV. *J. Am. Chem. Soc.* **2009**, *131*, 7220–7221.
37. Shichibu, Y.; Negishi, Y.; Tsukuda, T.; Teranishi, T. Large-Scale Synthesis of Thiolated Au_{25} Clusters *via* Ligand Exchange Reactions of Phosphine-Stabilized Au_{11} Clusters. *J. Am. Chem. Soc.* **2005**, *127*, 13464–13465.
38. Zhu, M.; Lanni, E.; Garg, N.; Bier, M. E.; Jin, R. Kinetically Controlled, High-Yield Synthesis of Au_{25} Clusters. *J. Am. Chem. Soc.* **2008**, *130*, 1138–1139.
39. Donkers, R. L.; Lee, D.; Murray, R. W. Synthesis and Isolation of the Molecule-like Cluster $Au_{38}(PhCH_2CH_2S)_{24}$. *Langmuir* **2004**, *20*, 1945–1952.
40. Habeeb Muhammed, M. A.; Pradeep, T. Au_{25}@SiO_2: Quantum Clusters of Gold Embedded in Silica. *Small* **2011**, *7*, 204–208.
41. Nimmala, P. R.; Dass, A. $Au_{36}(SPh)_{23}$ Nanomolecules. *J. Am. Chem. Soc.* **2011**, *133*, 9175–9177.
42. Chaki, N. K.; Negishi, Y.; Tsunoyama, H.; Shichibu, Y.; Tsukuda, T. Ubiquitous 8 and 29 kDa Gold:Alkanethiolate Cluster Compounds: Mass-Spectrometric Determination of Molecular Formulas and Structural Implications. *J. Am. Chem. Soc.* **2008**, *130*, 8608–8610.
43. Toikkanen, O.; Ruiz, V.; Ronholm, G.; Kalkkinen, N.; Liljeroth, P.; Quinn, B. M. Synthesis and Stability of Monolayer-Protected Au_{38} Clusters. *J. Am. Chem. Soc.* **2008**, *130*, 11049–11055.
44. Qian, H.; Zhu, Y.; Jin, R. Size-Focusing Synthesis, Optical and Electrochemical Properties of Monodisperse $Au_{38}(SC_2H_4Ph)_{24}$ Nanoclusters. *ACS Nano* **2009**, *3*, 3795–3803.
45. Jadzinsky, P. D.; Calero, G.; Ackerson, C. J.; Bushnell, D. A.; Kornberg, R. D. Structure of a Thiol Monolayer-Protected Gold Nanoparticle at 1.1 Å Resolution. *Science* **2007**, *318*, 430–433.
46. Qian, H.; Jin, R. Controlling Nanoparticles with Atomic Precision: The Case of $Au_{144}(SCH_2CH_2Ph)_{60}$. *Nano Lett.* **2009**, *9*, 4083–4087.
47. Qian, H.; Jin, R. Ambient Synthesis of $Au_{144}(SR)_{60}$ Nanoclusters in Methanol. *Chem. Mater.* **2011**, *23*, 2209–2217.
48. Heaven, M. W.; Dass, A.; White, P. S.; Holt, K. M.; Murray, R. W. Crystal Structure of the Gold Nanoparticle $[N(C_8H_{17})_4][Au_{25}(SCH_2CH_2Ph)_{18}]$. *J. Am. Chem. Soc.* **2008**, *130*, 3754–3755.
49. Zhu, M.; Aikens, C. M.; Hollander, F. J.; Schatz, G. C.; Jin, R. Correlating the Crystal Structure of a Thiol-Protected Au_{25} Cluster and Optical Properties. *J. Am. Chem. Soc.* **2008**, *130*, 5883–5885.
50. Zhu, M.; Eckenhoff, W. T.; Pintauer, T.; Jin, R. Conversion of Anionic $[Au_{25}(SCH_2CH_2Ph)_{18}]^-$ Cluster to Charge Neutral Cluster *via* Air Oxidation. *J. Phys. Chem. C* **2008**, *112*, 14221–14224.
51. Qian, H.; Eckenhoff, W. T.; Zhu, Y.; Pintauer, T.; Jin, R. Total Structure Determination of Thiolate-Protected Au_{38} Nanoparticles. *J. Am. Chem. Soc.* **2010**, *132*, 8280–8281.
52. Wu, Z.; Gayathri, C.; Gil, R. R.; Jin, R. Probing the Structure and Charge State of Glutathione-Capped $Au_{25}(SG)_{18}$ Clusters by NMR and Mass Spectrometry. *J. Am. Chem. Soc.* **2009**, *131*, 6535–6542.
53. Nair, P. M.; Roberts, J. D. Nuclear Magnetic Resonance Spectra. Hindered Rotation and Molecular Asymmetry. *J. Am. Chem. Soc.* **1957**, *79*, 4565–4566.
54. Parker, J. F.; Choi, J.-P.; Wang, W.; Murray, R. W. Electron Self-Exchange Dynamics of the Nanoparticle Couple $[Au_{25}(SC_2Ph)_{18}]^{0/1}$ by Nuclear Magnetic Resonance Line-Broadening. *J. Phys. Chem. C* **2008**, *112*, 13976–13981.
55. Venzo, A.; Antonello, S.; Gascon, J. A.; Guryanov, I.; Leapman, R. D.; Perera, N. V.; Sousa, A. A.; Zamuner, M.; Zanella, A.; Maran, F. Effect of the Charge State ($z = -1, 0, +1$) on the Nuclear Magnetic Resonance of Monodisperse $Au_{25}[S(CH_2)_2Ph]_{18}^z$ Clusters. *Anal. Chem.* **2011**, *83*, 6355.
56. Liu, Z.; Zhu, M.-Z.; Meng, X.; Xu, G.; Jin, R. Electron Transfer between $[Au_{25}(SC_2H_4Ph)_{18}]^-TOA^+$ and Oxoammonium Cations. *J. Phys. Chem. Lett.* **2011**, *2*, 2104–2109.
57. Wu, Z.; Jin, R. Stability of the Two Au–S Binding Modes in $Au_{25}(SG)_{18}$ Nanoclusters Probed by NMR and Optical Spectroscopy. *ACS Nano* **2009**, *3*, 2036–2042.
58. Zhu, M.; Qian, H.; Meng, X.; Jin, S.; Wu, Z.; Jin, R. Chiral Au_{25} Nanospheres and Nanorods: Synthesis and Insight into the Origin of Chirality. *Nano Lett.* **2011**, *11*, 3963–3969.